Anomalous electromagnetic scattering from radially anisotropic nanowires

H. L. Chen and L. Gao[*]

Jiangsu Key Laboratory of Thin Films, School of Physical Science and Technology, Soochow University, Suzhou 215006, China

We provide a full-wave electromagnetic (EM) scattering theory of discussing the electromagnetic scattering efficiency of radially anisotropic nanocylinders. In the long-wavelength limit, we derive the conditions for observing unusual EM scattering including non-Rayleigh vanishing and diverging ones. To verify our theoretical predictions, both full-wave numerical results and numerical simulations are performed, and good agreement is found. Moreover, physical origins of the anomalous phenomena are given. Therefore, the anisotropic nanowires under certain conditions can be hardly visible or exhibit superscattering. These results may find potential applications in different fields of nanotechnology.

I. INTRODUCTION

Light or electromagnetic scattering (EM) by small spherical particles (or cylindrical wires) is a fundamental problem in classical electrodynamics and was first quantitatively investigated by Rayleigh [1–3]. Later, exact solutions to the electromagnetic scattering of spherical particles were given by Mie, and a full-wave analysis was also established for the scattering of infinite cylinders, which is quite comparable to the Mie theory [4–7]. Recently, technological success in the fabrication of nanostructured materials has pushed the rapid development of nanotechnology, and the EM scattering cross section of the nanostructures may be made much smaller or larger than the geometrical cross section for EM cloaking [8,9] and for EM superscattering studies [10]. These studies on nanostructures may be useful for the various applications in many fields such as optical nanoantennas, optical cloaking, and optical manipulation.

In the Rayleigh limit, the traditional small nanosphere or nanocylinder can be regarded as an electric dipole or a line dipole, and the scattering efficiency Q_{sca} is dependent on the size parameter $q = k_0 a = \omega a/c$ (where k_0 is the wave vector in the vacuum and a is the radius of the sphere or the cylinder) with the form $Q_{sca} \sim q^4$ (for the sphere) or $Q_{sca} \sim q^3$ (for the cylinder), as $q \to 0$. However, for coated small spheres, by adjusting the optical properties of the core and the shell, the electric and magnetic dipole scattering can be made to vanish, and Q_{sca} was predicted to be proportional to q^8 [11]. Moreover, the EM scattering from the sphere made of negatively refractive materials could be constant, (i.e., $Q_{sca} \sim$ const) or even have inversionally proportional behavior with $Q_{sca} \sim 1/q^2$ [12,13]. Based upon the Mie theory, Lukýanchuk *et al.* studied the resonance scattering of small particles or thin wire with low dissipation rate and revealed anomalous EM scattering [14,15]. In addition, superscattering subwavelength nanostructructures can be designed by employing multiple resonances with almost the same frequency [16,17]. More recently, a doubly resonant structure was found to exhibit spectral behavior including both electromagnetic induced transparency and superscattering [18].

Physical studies on nanoparticles with radial anisotropy have also received much attention. Radial anisotropy requires

that the components of the permittivity and/or the permeability tensors of nanospheres be uniaxial in spherical coordinates with different values along the radial and tangential directions. For instance, this kind of anisotropy was taken into account to investigate the ultraviolet absorption and electron inelastic scattering cross section [19], the optical bistability [20], the invisibility of Pendry's cloak [21], the resonant coupling between localized plasmons and the radially anisotropic coatings [22], nonlinear susceptibilities for second and third harmonic generations [23,24], EM transparency [25], and surface enhanced Raman scattering [26]. Here we extend the full-wave EM theory for radially anisotropic spheres to radially anisotropic nanocylinders for the study of unusual scattering. The permittivity tensor $\overleftrightarrow{\varepsilon}$ and permeability tensor $\overleftrightarrow{\mu}$ are diagonal in cylinder coordinates (r,θ,z) [27–29], which is different from the anisotropy in Cartesian coordinates [30]. According to the full-wave electromagnetic theory and numerical simulations, we show that the scattering efficiency of the nanocylinder may take on unusual behavior such as $Q_{sca} \sim 1/q$ and $Q_{sca} \sim q^7$, in comparison with Rayleigh scattering $Q_{sca} \sim q^3$ [6].

The paper is organized as follows. In Sec. II, the full-wave electromagnetic theory is established for radially anisotropic nanocylinders. In Sec. III, in the long-wavelength limit, we derive the conditions for the Rayleigh and non-Rayleigh scattering. Numerical results are described in Sec. IV. Some conclusions and discussion are given in Sec. V.

II. FULL-WAVE ELECTROMAGNETIC THEORY

We consider the electromagnetic wave scattering from a radially anisotropic cylinder of radius a made of the material with relative permittivity tensor $\overleftrightarrow{\varepsilon}$ and relative permeability tensor $\overleftrightarrow{\mu}$ embedded into surrounding media with the relative permittivity ε_1 and relative permeability μ_1, as shown in Fig. 1. For radial anisotropy, the relative permittivity and permeability tensors are expressed as in cylindrical coordinates (r,θ,z) [27–29,31],

$$\overleftrightarrow{\varepsilon} = \begin{pmatrix} \varepsilon_r & 0 & 0 \\ 0 & \varepsilon_t & 0 \\ 0 & 0 & \varepsilon_z \end{pmatrix} \quad \text{and} \quad \overleftrightarrow{\mu} = \begin{pmatrix} \mu_r & 0 & 0 \\ 0 & \mu_t & 0 \\ 0 & 0 & \mu_z \end{pmatrix}. \quad (1)$$

Without loss of generality, the time dependence of a harmonic electromagnetic wave is assumed to be $e^{-i\omega t}$. Based on Maxwell equations, the time-independent part of local
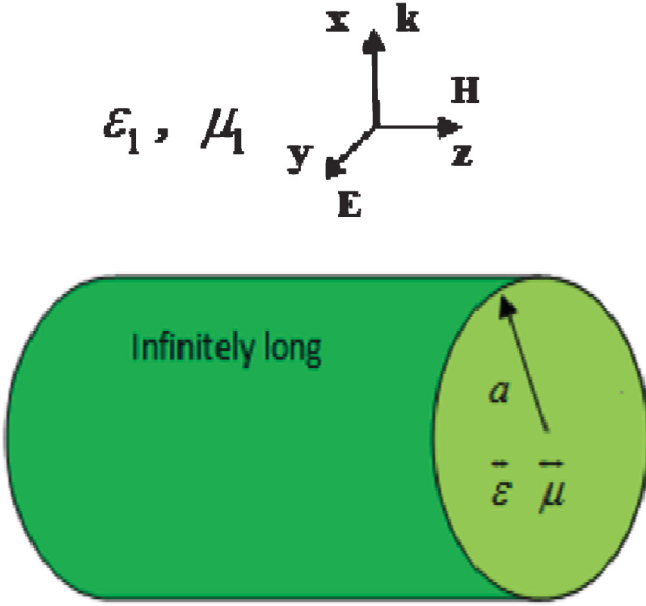
---

*leigao@suda.edu.cn

FIG. 1. (Color online) Geometry of a radially anisotropic cylinder. The incident wave propagates in the direction of **k**.

electric and magnetic fields can be written as

$$\nabla \times \mathbf{H} = -i\omega\varepsilon_0 \overleftrightarrow{\varepsilon} \, \mathbf{E}, \quad (2)$$

$$\nabla \times \mathbf{E} = i\omega\mu_0 \overleftrightarrow{\mu} \, \mathbf{H}, \quad (3)$$

where ε_0 and μ_0 are, respectively, the permittivity and permeability of vacuum. In cylindrical coordinates, Eqs. (2) and (3) become

$$\frac{1}{r}\frac{\partial H_z}{\partial \theta} - \frac{\partial H_\theta}{\partial z} = -i\omega\varepsilon_0\varepsilon_r E_r,$$

$$\frac{\partial H_r}{\partial z} - \frac{\partial H_z}{\partial r} = -i\omega\varepsilon_0\varepsilon_t E_\theta, \quad (4)$$

$$\frac{1}{r}\frac{\partial}{\partial r}(rH_\theta) - \frac{1}{r}\frac{\partial H_r}{\partial \theta} = -i\omega\varepsilon_0\varepsilon_z E_z,$$

and

$$\frac{1}{r}\frac{\partial E_z}{\partial \theta} - \frac{\partial E_\theta}{\partial z} = i\omega\mu_0\mu_r H_r,$$

$$\frac{\partial E_r}{\partial z} - \frac{\partial E_z}{\partial r} = i\omega\mu_0\mu_t H_\theta, \quad (5)$$

$$\frac{1}{r}\frac{\partial}{\partial r}(rE_\theta) - \frac{1}{r}\frac{\partial E_r}{\partial \theta} = i\omega\mu_0\mu_z H_z.$$

When a transverse-magnetic (TM) incident wave, defined by a wave vector **k**, with its magnetic field polarized along the z direction, impinges on the anisotropic cylinder, we have $H_r = 0$ and $H_\theta = 0$. In this situation, with Eqs. (4) and (5), the magnetic field H_z can be written as

$$\frac{1}{r}\left[\frac{\partial}{\partial r}\left(\frac{r}{\varepsilon_t}\frac{\partial H_z}{\partial r}\right)\right] + \frac{1}{r^2}\frac{\partial}{\partial \theta}\left(\frac{1}{\varepsilon_r}\frac{\partial H_z}{\partial \theta}\right) + k_0^2\mu_z H_z = 0. \quad (6)$$

Inserting the solutions of the form $H_z = \Phi(r)\,\Theta(\theta)$ into the above equation, we get

$$\frac{d^2\Theta}{d\theta^2} + n^2\Theta = 0, \quad (7)$$

$$r^2\frac{d^2\Phi}{dr^2} + r\frac{d\Phi}{dr} + \left(k_0^2\varepsilon_t\mu_z r^2 - n^2\frac{\varepsilon_t}{\varepsilon_r}\right)\Phi = 0. \quad (8)$$

For the incident TM wave, the incident magnetic field H_z can be expanded as $H_z = \sum_{n=-\infty}^{\infty} i^n J_n(k_0 r)e^{in\theta}$, where $J_n(\dots)$ is the nth-order Bessel function. Note that Eq. (7) admits the solutions $\Theta(\theta) \sim e^{\pm in\theta}$ ($n = 0, \pm 1, \pm 2, \dots$) and Eq. (8) is a generalized Bessel equation.

When n' ($\equiv n\sqrt{\varepsilon_t}/\sqrt{\varepsilon_r}$) is an integer, the solutions for Eq. (6) inside and outside of the anisotropic cylinder are expressed as

$$H_z^{\text{in}} = \sum_{n=-\infty}^{+\infty} i^n c_n J_{n'}(k_2 r)e^{in\theta}, \quad r < a,$$

$$H_z^{\text{out}} = \sum_{n=-\infty}^{\infty} i^n[J_n(k_1 r) + b_n H_n(k_1 r)]e^{in\theta}, \quad r > a,$$

(9)

where $k_1 = \sqrt{\varepsilon_1}\sqrt{\mu_1}k_0$, $k_2 = \sqrt{\varepsilon_t}\sqrt{\mu_z}k_0$, $H_n(\dots)$ is the nth-order Hankel function of the first kind, and b_n, c_n are the undetermined coefficients. For absorptive magnetodielectric materials, the imaginary part of the components of permittivity and permeability tensors such as $\varepsilon_{r(t)}$ and $\mu_{r(t)}$ are positive, and their square roots should be chosen to keep both the imaginary part of the relative refractive index $n_p = \sqrt{\varepsilon_t}\sqrt{\mu_z}$ and the real part of wave impedance $Z = \sqrt{\mu_z}\sqrt{\mu_0}/(\sqrt{\varepsilon_t}\sqrt{\varepsilon_0})$ positive. For more details, we refer the readers to Refs. [32,33].

If the boundary conditions are that E_θ and H_z are continuous at $r = a$, we can derive the scattering coefficient b_n,

$$b_n = -\frac{\sqrt{\varepsilon_t}/\sqrt{\varepsilon_1}J_n'(k_1 a)J_{n'}(k_2 a) - \sqrt{\mu_z}/\sqrt{\mu_1}J_n(k_1 a)J_{n'}'(k_2 a)}{\sqrt{\varepsilon_t}/\sqrt{\varepsilon_1}H_n'(k_1 a)J_{n'}(k_2 a) - \sqrt{\mu_z}\sqrt{\mu_1}H_n(k_1 a)J_{n'}'(k_2 a)} \quad (n = 0, \pm 1, \dots). \quad (10)$$

Equation (10) reduces to the scattering coefficient for the isotropic cylinder [6]. However, when n' ($\equiv n\sqrt{\varepsilon_t}/\sqrt{\varepsilon_r}$) is not an integer, the solutions inside and outside of the cylinder should be described as

$$H_z^{\text{in}} = \sum_{n=-\infty}^{-1} i^n c_n J_{-n'}(k_2 r)e^{in\theta} + \sum_{n=0}^{\infty} i^n d_n J_{n'}(k_2 r)e^{in\theta}, \quad r < a, \quad H_z^{\text{out}} = \sum_{n=-\infty}^{\infty} i^n[J_n(k_1 r) + b_n H_n(k_1 r)]e^{in\theta}, \quad r > a.$$

(11)

Then, one obtains

$$
b_n = \begin{cases} -\dfrac{\sqrt{\varepsilon_t}/\sqrt{\varepsilon_1}J'_n(k_1a)J_{n'}(k_2a)-\sqrt{\mu_z}/\sqrt{\mu_1}J_n(k_1a)J'_{n'}(k_2a)}{\sqrt{\varepsilon_t}/\sqrt{\varepsilon_1}H'_n(k_1a)J_{n'}(k_2a)-\sqrt{\mu_z}/\sqrt{\mu_1}H_n(k_1a)J'_{n'}(k_2a)} & (n \geqslant 0), \\[2ex] -\dfrac{\sqrt{\varepsilon_t}/\sqrt{\varepsilon_1}J'_n(k_1a)J_{-n'}(k_2a)-\sqrt{\mu_z}/\sqrt{\mu_1}J_n(k_1a)J'_{-n'}(k_2a)}{\sqrt{\varepsilon_t}/\sqrt{\varepsilon_1}H'_n(k_1a)J_{-n'}(k_2a)-\sqrt{\mu_z}/\sqrt{\mu_1}H_n(k_1a)J'_{-n'}(k_2a)} & (n < 0). \end{cases} \tag{12}
$$

Similarly, for the transverse-electric field, the scattering coefficient a_n can be written as

$$
a_n = -\frac{\sqrt{\mu_t}/\sqrt{\mu_1}J'_n(k_1a)J_{n'}(k_2a)-\sqrt{\varepsilon_z}/\sqrt{\varepsilon_1}J_n(k_1a)J'_{n'}(k_2a)}{\sqrt{\mu_t}/\sqrt{\mu_1}H'_n(k_1a)J_{n'}(k_2a)-\sqrt{\varepsilon_z}/\sqrt{\varepsilon_1}H_n(k_1a)J'_{n'}(k_2a)} \tag{13}
$$

for an integer $n'\,(\equiv n\sqrt{\mu_t}/\sqrt{\mu_r})$, and

$$
a_n = \begin{cases} -\dfrac{\sqrt{\mu_t}/\sqrt{\mu_1}J'_n(k_1a)J_{n'}(k_2a)-\sqrt{\varepsilon_z}/\sqrt{\varepsilon_1}J_n(k_1a)J'_{n'}(k_2a)}{\sqrt{\mu_t}/\sqrt{\mu_1}H'_n(k_1a)J_{n'}(k_2a)-\sqrt{\varepsilon_z}/\sqrt{\varepsilon_1}H_n(k_1a)J'_{n'}(k_2a)} & (n \geqslant 0), \\[2ex] -\dfrac{\sqrt{\mu_t}/\sqrt{\mu_1}J'_n(k_1a)J_{-n'}(k_2a)-\sqrt{\varepsilon_z}/\sqrt{\varepsilon_1}J_n(k_1a)J'_{-n'}(k_2a)}{\sqrt{\mu_t}/\sqrt{\mu_1}H'_n(k_1a)J_{-n'}(k_2a)-\sqrt{\varepsilon_z}/\sqrt{\varepsilon_1}H_n(k_1a)J'_{-n'}(k_2a)} & (n < 0), \end{cases} \tag{14}
$$

for a noninteger n', with $k_2 = \sqrt{\varepsilon_z}\sqrt{\mu_t}k_0$. Here we mention that regardless of whether n' is an integer, these coefficients are symmetrical, that is, $a_n = a_{-n}$ and $b_n = b_{-n}$ for $n > 0$.

The scattering efficiency Q_{sca} is defined as [15]

$$
Q_{\text{sca}} = \frac{2}{k_1a}\sum_{n=-\infty}^{\infty}|b_n|^2 \quad \text{(for TM wave)}, \tag{15}
$$

$$
Q_{\text{sca}} = \frac{2}{k_1a}\sum_{n=-\infty}^{\infty}|a_n|^2 \quad \text{(for TE wave)}. \tag{16}
$$

III. RAYLEIGH AND NON-RAYLEIGH SCATTERING IN THE LONG-WAVELENGTH REGION

In this section, we consider the long-wavelength limit or small cylindrical case, that is, $k_1a = \sqrt{\varepsilon_1}\sqrt{\mu_1}\omega a/c = \sqrt{\varepsilon_1}\sqrt{\mu_1}q \ll 1$ and $k_2a = \sqrt{\varepsilon_t}\sqrt{\mu_z}\omega a/c = \sqrt{\varepsilon_t}\sqrt{\mu_z}q \ll 1$. In this connection, Eq. (15) converges very fast, and the effective scattering from the anisotropic cylinder is mainly determined by $n=0$ and $n=\pm 1$ terms. Let us express the scattering coefficients b_0 and b_1 $(b_{-1}=b_1)$ for TM polarization as [14]

$$
b_n = -R_n(R_n + iS_n), \tag{17}
$$

with

$$
\begin{aligned}
R_n &= \sqrt{\varepsilon_t}/\sqrt{\varepsilon_1}J'_n(\sqrt{\varepsilon_1}\sqrt{\mu_1}q)J_{n'}(\sqrt{\varepsilon_t}\sqrt{\mu_z}q) \\
&\quad - \sqrt{\mu_z}/\sqrt{\mu_1}J_n(\sqrt{\varepsilon_1}\sqrt{\mu_1}q)J'_{n'}(\sqrt{\varepsilon_t}\sqrt{\mu_z}q), \\
S_n &= \sqrt{\varepsilon_t}/\sqrt{\varepsilon_1}Y'_n(\sqrt{\varepsilon_1}\sqrt{\mu_1}q)J_{n'}(\sqrt{\varepsilon_t}\sqrt{\mu_z}q) \\
&\quad - \sqrt{\mu_z}/\sqrt{\mu_1}Y_n(\sqrt{\varepsilon_1}\sqrt{\mu_1}q)J'_{n'}(\sqrt{\varepsilon_t}\sqrt{\mu_z}q),
\end{aligned}
$$

where $Y_n(\dots)$ is the nth-order Neumann function. For the small cylindrical case, the relevant functions admit a simple form,

$$
J_0(x) \approx 1 - \left(\frac{x}{2}\right)^2 + \frac{1}{4}\left(\frac{x}{2}\right)^4, \quad J_1(x) \approx \frac{x}{2} - \frac{1}{2}\left(\frac{x}{2}\right)^3,
$$

$$
Y_0(x) \approx \frac{2}{\pi}\ln\frac{x}{2}, \quad Y_1(x) \approx -\frac{2}{\pi x}. \tag{18}
$$

On the other hand, for a noninteger n', we adopt

$$
J_{n'}(x) \approx \left(\frac{x}{2}\right)^{n'}\left[\frac{1}{\Gamma(n'+1)} - \frac{1}{\Gamma(n'+2)}\left(\frac{x}{2}\right)^2 \right.
$$
$$
\left. + \frac{1}{2\Gamma(n'+3)}\left(\frac{x}{2}\right)^4\right],
$$
$$
J'_{n'}(x) = J_{n'-1}(x) - \frac{n'}{x}J_{n'}(x), \tag{19}
$$

where $\Gamma(\dots)$ is the Euler γ function.

Thus, for b_0, we have

$$
\begin{aligned}
R_0 &= \left(-\sqrt{\varepsilon_t}\sqrt{\mu_1} + \frac{\mu_z\sqrt{\varepsilon_t}}{\sqrt{\mu_1}}\right)\left(\frac{q}{2}\right) \\
&\quad + \left[\frac{1}{2}\left(\varepsilon_1\mu_1^{3/2}\sqrt{\varepsilon_t} - \frac{\mu_z^2\varepsilon_t^{3/2}}{\sqrt{\mu_1}}\right)\right. \\
&\quad \left. + \left(\varepsilon_t^{3/2}\sqrt{\mu_1}\mu_z - \varepsilon_1\mu_z\sqrt{\mu_1}\sqrt{\varepsilon_t}\right)\right]\left(\frac{q}{2}\right)^3,
\end{aligned}
$$
$$
S_0 = \frac{\sqrt{\varepsilon_t}}{\varepsilon_1\sqrt{\mu_1}}\frac{2}{\pi q}, \tag{20}
$$

and

$$
\begin{aligned}
R_1 &= \frac{1}{\Gamma(\sqrt{\varepsilon_t}/\sqrt{\varepsilon_r})}\left(\frac{\sqrt{\varepsilon_t}\sqrt{\mu_z}}{2}q\right)^{\sqrt{\varepsilon_t}/\sqrt{\varepsilon_r}}\left\{\frac{1}{2}\left(\frac{\sqrt{\varepsilon_r}}{\sqrt{\varepsilon_1}} - \frac{\sqrt{\varepsilon_1}}{\sqrt{\varepsilon_t}}\right)\right. \\
&\quad + \left[\frac{\sqrt{\varepsilon_1}\sqrt{\varepsilon_r}\mu_z}{4} + \frac{\varepsilon_1^{3/2}\mu_1}{16\sqrt{\varepsilon_t}} - \frac{3\mu_1\sqrt{\varepsilon_1}\sqrt{\varepsilon_r}}{16}\right. \\
&\quad \left.\left. - \frac{\sqrt{\varepsilon_1}\sqrt{\varepsilon_t}\mu_z + \sqrt{\varepsilon_r}\varepsilon_t\mu_z/\sqrt{\varepsilon_1}}{8(\sqrt{\varepsilon_t}/\sqrt{\varepsilon_r}+1)}\right]q^2\right\}, \\
S_1 &= \frac{1}{\Gamma(\sqrt{\varepsilon_t}/\sqrt{\varepsilon_r})}\left(\frac{\sqrt{\varepsilon_t}\sqrt{\mu_z}}{2}q\right)^{\sqrt{\varepsilon_t}/\sqrt{\varepsilon_r}}\left\{\left(\frac{2}{\pi q^2}\right)\right. \\
&\quad \times \left(\frac{\sqrt{\varepsilon_r}}{\varepsilon_1^{3/2}\mu_1} + \frac{1}{\sqrt{\varepsilon_1}\mu_1\sqrt{\varepsilon_t}}\right) - \frac{\sqrt{\varepsilon_r}\mu_z}{\pi\sqrt{\varepsilon_1}\mu_1} \\
&\quad \left. + \frac{\mu_z\sqrt{\varepsilon_t}/(\sqrt{\varepsilon_1}\mu_1) - \varepsilon_t\mu_z\sqrt{\varepsilon_r}/(\mu_1\varepsilon_1^{3/2})}{2\pi(\sqrt{\varepsilon_t}/\sqrt{\varepsilon_r}+1)}\right\}, \tag{21}
\end{aligned}
$$

for b_1.

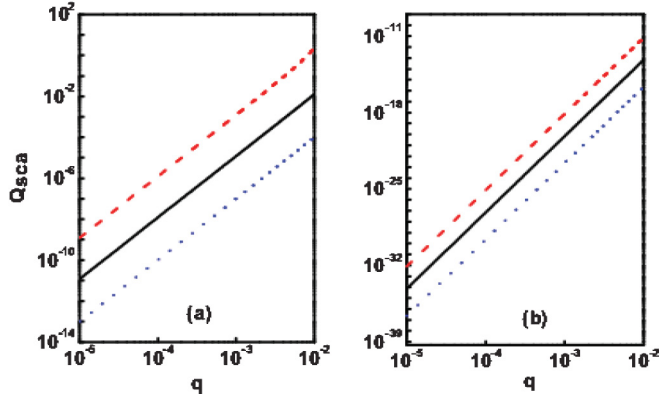(1) The Rayleigh case: Generally, after keeping the leading

FIG. 2. (Color online) (a) Log-log plot of the scattering efficiency vs size parameter q. (a) $\mu_z = 10$ (blue dotted line), $\mu_z = 100$ (black solid line), and $\mu_z = 1000$ (red dashed line). Other parameters are $\varepsilon_r = 0.5$ and $\varepsilon_t = 2$. (b) $\mu_z = 1$ and $\sqrt{\varepsilon_r}\sqrt{\varepsilon_t} = 1$ such as $\varepsilon_r = 0.5$, $\varepsilon_t = 2$ (blue dotted line), $\varepsilon_r = 0.05$, $\varepsilon_t = 20$ (black solid line), and $\varepsilon_r = 0.005$, $\varepsilon_t = 200$ (red dashed line).

orders in $R_{0(1)}$ and $S_{0(1)}$, we have

$$b_0 \approx i\frac{\pi}{4}(\mu_z - \mu_1)\varepsilon_1 q^2 \quad \text{and}$$

$$b_1 \approx i\frac{\pi}{4}\frac{(\sqrt{\varepsilon_r}/\sqrt{\varepsilon_1} - \sqrt{\varepsilon_1}/\sqrt{\varepsilon_t})}{1/(\mu_1\sqrt{\varepsilon_1}\sqrt{\varepsilon_t}) + \sqrt{\varepsilon_r}/(\varepsilon_1^{3/2}\mu_1)}q^2. \tag{22}$$

The substitution of above equation into the Eq. (15) leads to

$$Q_{\text{sca}} \approx \frac{q^3}{8\sqrt{\varepsilon_1}\sqrt{\mu_1}}\left\{2\left|\frac{(\sqrt{\varepsilon_r}/\sqrt{\varepsilon_1} - \sqrt{\varepsilon_1}/\sqrt{\varepsilon_t})\pi}{\sqrt{\varepsilon_r}/(\varepsilon_1^{\frac{3}{2}}\mu_1) + 1/(\sqrt{\varepsilon_1}\mu_1\sqrt{\varepsilon_t})}\right|^2 \right.$$
$$\left. + \pi^2|(\mu_z - \mu_1)\varepsilon_1|^2 \right\}, \tag{23}$$

which is quite similar as the behavior for the scattering efficiency for isotropic nanocylinders such as $Q_{\text{sca}} \sim q^3$. In other words, with decreasing q, the scattering efficiency is decreased and should vanish as $q \to 0$, as expected.

(2) The non-Rayleigh vanishing case: If we let $\mu_z = \mu_1$, the first term in R_0 vanishes, and higher order in q should be taken into account. At the same time, when $\sqrt{\varepsilon_r}\sqrt{\varepsilon_t} = \varepsilon_1$, the first term in R_1 vanishes, and the second term for q^4 should be considered. As a result, we arrive at

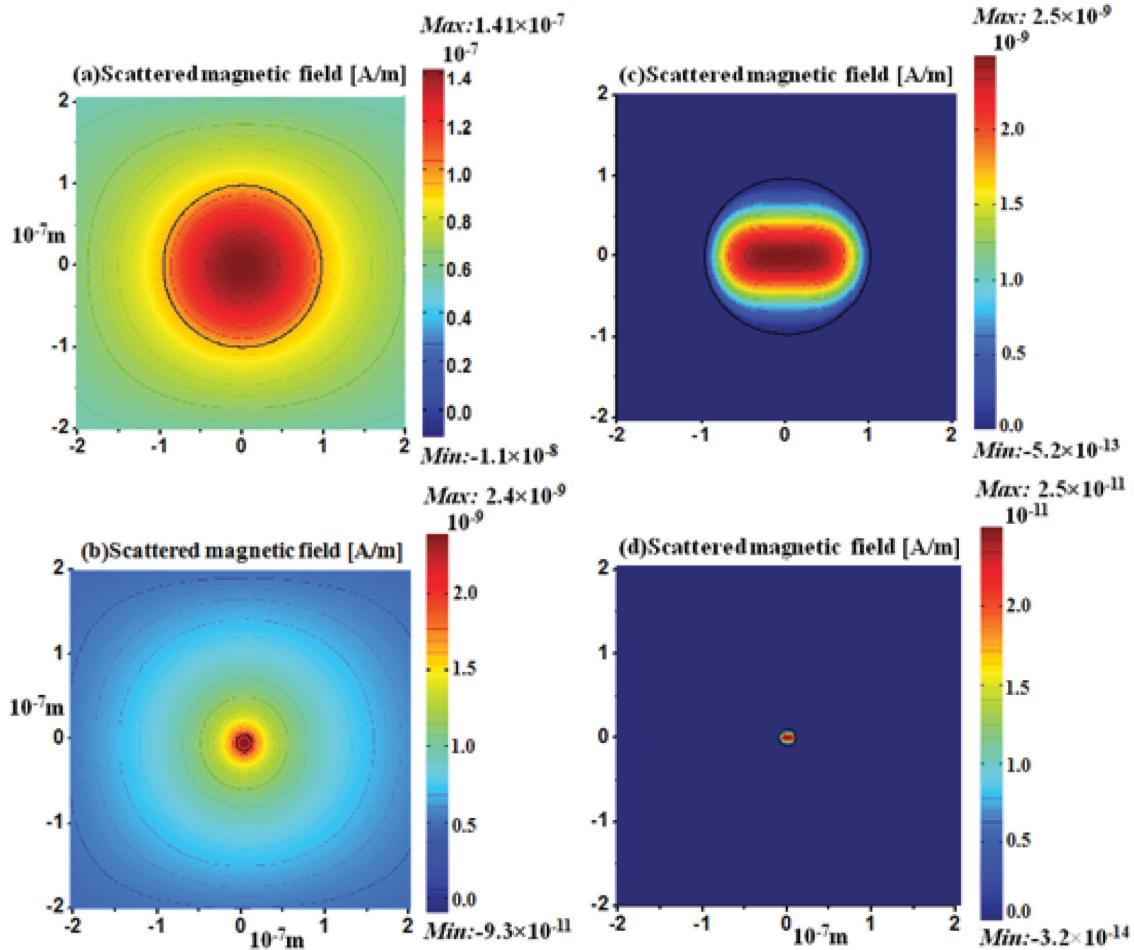$$b_0 = i\pi\frac{\varepsilon_1\mu_1^2(\varepsilon_t - \varepsilon_1)}{32}q^4 \quad \text{and}$$

FIG. 3. (Color online) The distribution of the magnetic fields both inside and outside of the anisotropic cylinder for $\varepsilon_r = 0.5$ and $\varepsilon_t = 2$ ($\sqrt{\varepsilon_r}\sqrt{\varepsilon_t} = 1$) for Rayleigh behavior: (a) $q = 0.001$ and $\mu_z = 10$; (b) $q = 0.0001$ and $\mu_z = 10$. For non-Rayleigh vanishing behavior: (c) $q = 0.001$ and $\mu_z = 1$, (d) $q = 0.0001$ and $\mu_z = 1$.

$$b_1 = i\frac{\pi}{16}\left(\frac{\varepsilon_1^2\mu_1^2}{2} + \frac{\varepsilon_1^2\mu_1^2\varepsilon_t}{\varepsilon_1 + \varepsilon_t}\right)q^4. \tag{24}$$

Then, one obtains

$$Q_{\text{sca}} \approx \frac{\pi^2 q^7}{512\sqrt{\varepsilon_1}\sqrt{\mu_1}}\left[2\left|\varepsilon_1^2\mu_1^2 + \frac{2\varepsilon_1\mu_1^2\varepsilon_t}{(\varepsilon_t/\varepsilon_1 + 1)}\right|^2\right.$$
$$\left. + \left|\varepsilon_1\mu_1^2(\varepsilon_t - \varepsilon_1)\right|^2\right]. \tag{25}$$

In this case, one observes the unusual dependence of Q_{sca} on q; that is, $Q_{\text{sca}} \sim q^7$. As $q \to 0$, one may observe that Q_{sca} should vanish much faster than the one for the Rayleigh case. Therefore, it is possible to realize faster vanishing of the scattering efficiency with the anisotropic cylinders, resulting in better transparency than with isotropic cylinders.

(3) The non-Rayleigh diverging case: If the condition $\sqrt{\varepsilon_r}\sqrt{\varepsilon_t} = -\varepsilon_1$ is satisfied, we have

$$b_0 = i\frac{\pi(\mu_z - \mu_1)\varepsilon_1}{4}q^2 \quad \text{and}$$

$$b_1 = \frac{1}{i\{\mu_z/(\pi\mu_1) + \varepsilon_t\mu_z/[\pi\mu_1(\varepsilon_1 - \varepsilon_t)]\} - 1}. \tag{26}$$

Then, one observes the other unusual behavior, that is,

$$Q_{\text{sca}} \approx \frac{4}{\sqrt{\varepsilon_1}\sqrt{\mu_1}}\frac{1}{q}\frac{1}{1 + |\mu_z/(\pi\mu_1) + \varepsilon_t\mu_z/[\pi\mu_1(\varepsilon_1 - \varepsilon_t)]|^2}. \tag{27}$$

In contrast to the above vanishing behavior of Q_{sca} with decreasing q, we expect to observe the divergence of Q_{sca} as $q \to 0$.

Moreover, we can resort to the effective medium theory in the long-wavelength limit. That is to say, the anisotropic cylindrical nanowire can be regarded as an equivalent one with isotropic effective permittivity ε_e and permeability μ_e [29]. To derive them, we replace ε_1 and μ_1 with ε_e and μ_e in the dominant scattering coefficients b_0 and b_1 for TM polarization, and let b_0 and b_1 equal zero [34]. We then have

$$\sqrt{\varepsilon_t}/\sqrt{\varepsilon_e}J_0'(k_ea)J_0(k_2a) - \sqrt{\mu_z}/\sqrt{\mu_e}J_0(k_ea)J_0'(k_2a) = 0, \tag{28}$$

$$\sqrt{\varepsilon_t}/\sqrt{\varepsilon_e}J_1'(k_ea)J_{\sqrt{\varepsilon_t}/\sqrt{\varepsilon_r}}(k_2a)$$
$$- \sqrt{\mu_z}/\sqrt{\mu_e}J_1(k_ea)J_{\sqrt{\varepsilon_t}/\sqrt{\varepsilon_r}}'(k_2a) = 0, \tag{29}$$

with $k_e = \sqrt{\varepsilon_e}\sqrt{\mu_e}\omega/c$. Using Eqs. (18) and (19), we obtain

$$\mu_e = \mu_z \quad \text{and} \quad \varepsilon_e = \sqrt{\varepsilon_r}\sqrt{\varepsilon_t}. \tag{30}$$

IV. NUMERICAL RESULTS

To verify our analytical theory, we numerically calculate the scattering efficiency with the full-wave electromagnetic theory based on Eqs. (10), (12), and (15). For simplify, we consider that the surrounding media is a vacuum with $\varepsilon_1 = \mu_1 = 1$, and then we have $k_1a = q$ and $k_2a = \sqrt{\varepsilon_t}\sqrt{\mu_z}q$.

With our full-wave EM theory, we first study two cases in which the scattering efficiencies exhibits the vanishing behavior when q tends to zero, as shown in Fig. 2. We find that for ordinary anisotropic physical parameters, the
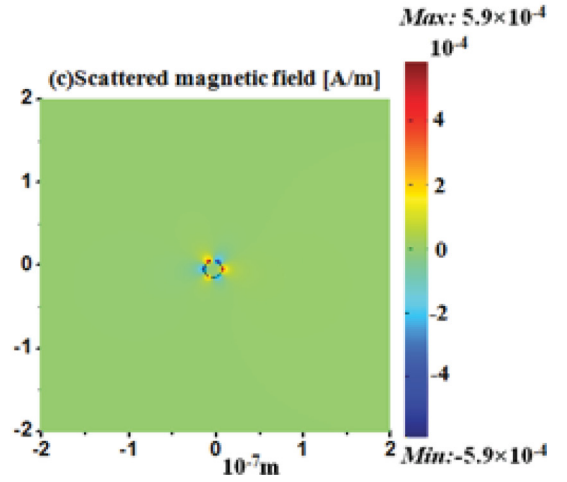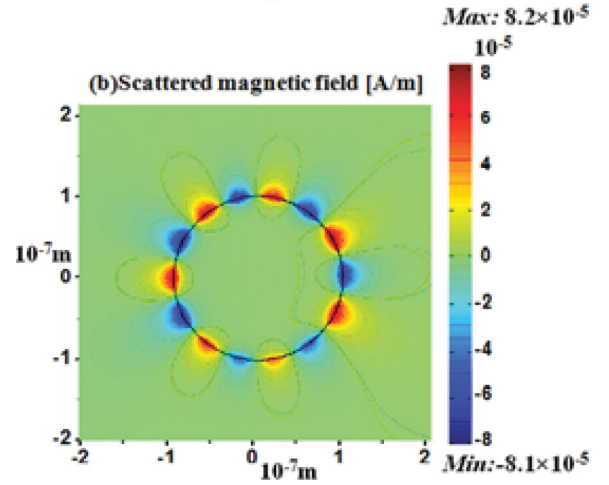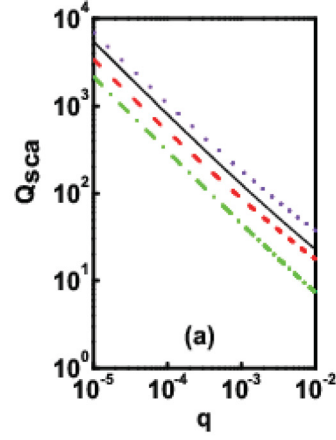

FIG. 4. (Color online) (a) Log-log plot of the scattering efficiency vs size parameter q for different parameters: (i) $\varepsilon_r = -0.5$, $\varepsilon_t = -2$, and $\mu_z = 1$ (violet dotted line), (ii) $\varepsilon_r = -0.5$, $\varepsilon_t = -2$, and $\mu_z = 10$ (black solid line), (iii) $\varepsilon_r = -2$, $\varepsilon_t = -0.5$, and $\mu_z = 1$ (red dashed line), and (iv) $\varepsilon_r = -2$, $\varepsilon_t = -0.5$, and $\mu_z = 10$ (green dashed and dotted line). Distributions of the magnetic field: (b) $q = 0.001$ and (c) $q = 0.0001$. Other parameters are $\varepsilon_r = -0.5$, $\varepsilon_t = -2$, and $\mu_z = 1$.

scattering efficiency obeys the Rayleigh law $Q_{\text{sca}} \sim q^3$ [see Fig. 2(a)]. However, for $\sqrt{\varepsilon_r}\sqrt{\varepsilon_t} = \varepsilon_1 = 1$ and $\mu_z = \mu_1 = 1$, Q_{sca} exhibits a fast decrease with decreasing q and obeys unusual scattering $Q_{\text{sca}} \sim q^7$ [see Fig. 2(b)]. Hence, those asymptotic behavior of all curves is consistent with our
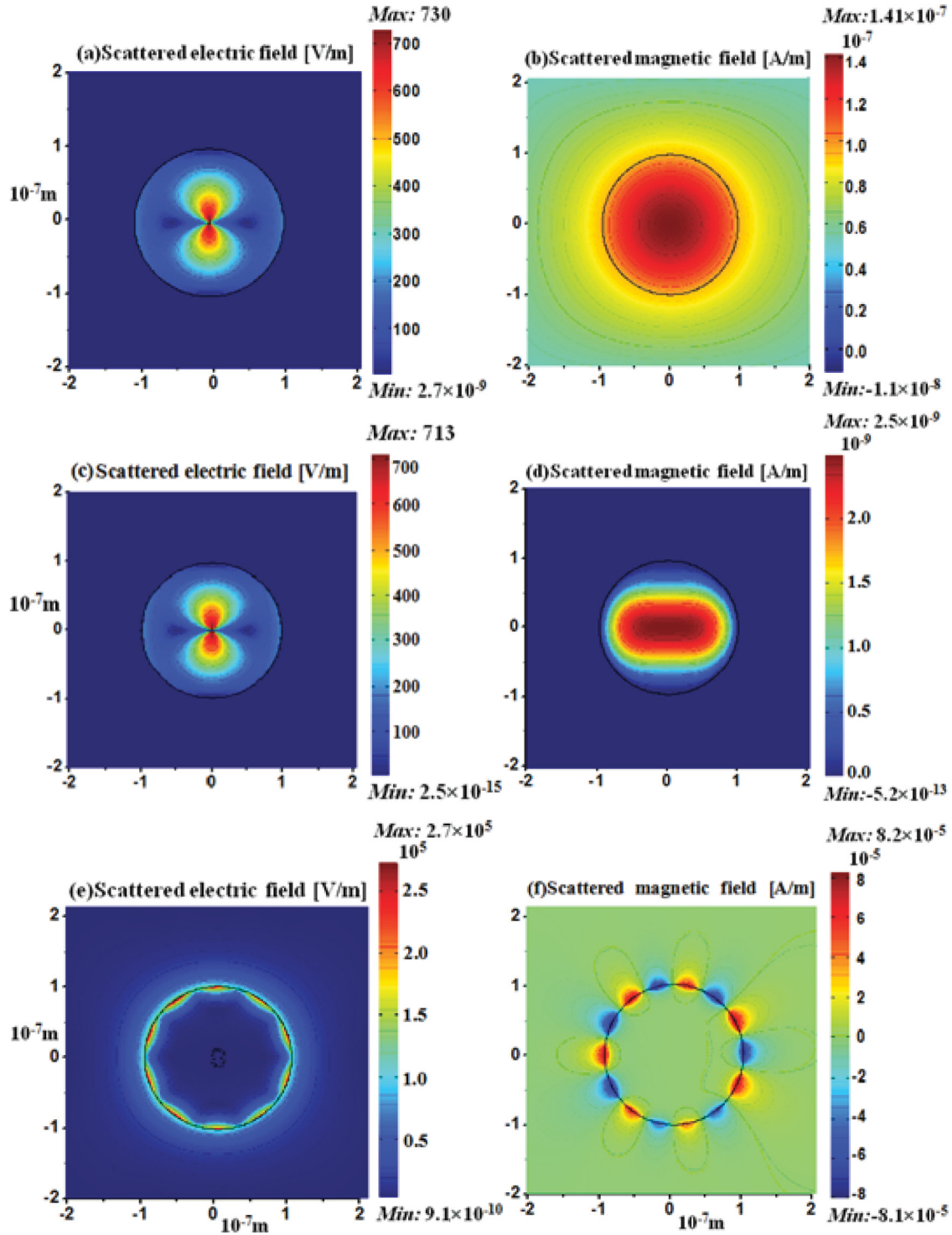
FIG. 5. (Color online) The distribution of the electric [(a), (c), and (e)] and magnetic [(b), (d), and (f)] fields for $q = 0.001$: (a) and (b) Rayleigh vanishing behavior for $\varepsilon_r = 0.5$, $\varepsilon_t = 2$, and $\mu_z = 10$; (c) and (d) non-Rayleigh vanishing behavior for $\varepsilon_r = 0.5$, $\varepsilon_t = 2$, and $\mu_z = 1$; and (e) and (f) non-Rayleigh diverging behavior for $\varepsilon_r = -0.5$, $\varepsilon_t = -2$, and $\mu_z = 1$.

analytical predictions. Moreover, from Fig. 2(b), one can obtain much lower Q_{sca} by the suitable adjustment of the radial anisotropy.

In Fig. 3, we perform the Comsol multiphysics simulation to calculate the distribution of the magnetic field inside and outside the anisotropic cylinders for Rayleigh and non-

Rayleigh vanishing cases. For both Rayleigh [see Figs. 3(a) and 3(b)] and non-Rayleigh [see Figs. 3(c) and 3(d)] cases, one clearly observes that the outside scattering magnetic fields becomes weak with decreasing the size parameter q, as expected. Moreover, the scattering magnetic fields under the non-Rayleigh condition (see the right column) are much

weaker than those under the Rayleigh condition (see the left column). Physically, the anisotropic nanocylinder acts as a magnetic monopole under the Rayleigh condition, while it acts as a magnetic dipole for the non-Rayleigh case. Actually, according to our anisotropic effective medium theory, under non-Rayleigh conditions, anisotropic nanocylinders can be regarded as isotropic with the effective permittivity $\varepsilon_e = 1$ and the effective permeability $\mu_e = 1$ [29]. In other words, such anisotropic cylindrical scatter behaves as that of an isotropic cylinder made of a vacuum. As a consequence, one may observe much suppressed scattering efficiency [11,35].

In Fig. 4, we investigate the scattering efficiency based on the full-wave solutions and the corresponding distribution of fields based on the Comsol simulation under the non-Rayleigh diverging condition $\sqrt{\varepsilon_r}\sqrt{\varepsilon_t} = -1$. It is evident that Q_{sca} exhibits anomalous superscattering such as $Q_{\text{sca}} \sim q^{-1}$ instead of Rayleigh scattering $Q_{\text{sca}} \sim q^3$. In detail, Q_{sca} is increased with the reduction of the size parameter q. Note that the total scattering cross section in this case $\sigma_{\text{sca}} \sim Q_{\text{sca}}q$ is still independent of q. From the near-field diagram [see Figs. 4(b) and 4(c)], we further find that the scattering magnetic field is large for small q and the field-enhancement is concentrated on the surface of nanocylinders. The strong field localization is a result of surface plasmon electric resonance. Actually, for isotropic cylinders, the surface plasmon resonances take places at $\varepsilon_2 + \varepsilon_1 = 0$, where ε_2 is the permittivity of the isotropic cylinder. For radially anisotropic cylinders, the surface plasmon resonance arises at $\sqrt{\varepsilon_r}\sqrt{\varepsilon_t} + \varepsilon_1 = 0$, which can be easily understood because the effective permittivity of the anisotropic cylinder ε_e equals $\sqrt{\varepsilon_r}\sqrt{\varepsilon_t}$.

In the end, we aim to study the original physics in the asymptotic behavior of the scattering efficiency as $q \to 0$. For this purpose, we plot the distributions of both electric and magnetic fields for the Rayleigh case, the non-Rayleigh vanishing case, and the non-Rayleigh diverging case in Fig. 5. Under the Rayleigh and non-Rayleigh vanishing conditions, it turns out that the distribution of the electric fields is almost the same and resembles the electric dipole excitation [see Figs. 5(a) and 5(c)]. However, the distribution of the magnetic fields is quite different, although the magnitude of the magnetic fields is very weak. The anisotropic cylinder behaves as a magnetic monopole for the Rayleigh case [see Fig. 5(b)], whereas it is treated as a magnetic dipole for the non-Rayleigh vanishing case [see Fig. 5(d)]. The magnitude of the scattering magnetic field for non-Rayleigh case is about five orders less than that of the one for Rayleigh case and is almost zero. Therefore, under the non-Rayleigh vanishing condition, the radially anisotropic cylinder is almost transparent. On the

other hand, under the non-Rayleigh diverging condition that $\sqrt{\varepsilon_r}\sqrt{\varepsilon_t} + 1 = 0$ [see Figs. 5(e) and 5(f)], surface plasmon electric resonance produces large enhancement of electric field and corresponding enhancement of the magnetic field near the interface between the anisotropic cylinder and the air, resulting in the anomalous superscattering.

V. CONCLUSIONS

In this paper, we develop a full-wave electromagnetic theory to investigate the EM scattering from radially anisotropic nanocylinders. Under certain conditions, both analytical and numerical results show that the scattering efficiency Q_{sca} can exhibit non-Rayleigh vanishing asymptotic behavior ($Q_{\text{sca}} \sim q^7$) and non-Rayleigh diverging behavior ($Q_{\text{sca}} \sim 1/q$) instead of the traditional Rayleigh scattering ($Q_{\text{sca}} \sim q^3$) as $q \to 0$. Under non-Rayleigh vanishing conditions $\sqrt{\varepsilon_r}\sqrt{\varepsilon_e} = \varepsilon_1$ and $\mu_z = \mu_1$, the anisotropic cylinders exhibit abnormally low EM scattering section and hence are almost transparent. On the other hand, for $\sqrt{\varepsilon_r}\sqrt{\varepsilon_t} = -1$, the surface electric plasmon resonance arises and scattering electric and magnetic fields are enhanced, resulting in superscattering efficiency. Therefore, our study may provide insight into the general electromagnetic properties of anisotropic nanoparticles and nanometamaterials.

Some comments are in order. The unusual behavior we obtained is related to nondissipative cases. In real dissipative systems where $\text{Im}(\varepsilon_i)$ or $\text{Im}(\mu_i)$ is not zero, it is difficult to observe the reported non-Rayleigh behavior [12,13]. Our preliminary studies show that it is still possible to observe such unusual behavior if the absorptive terms are smaller than the critical ones, dependent on the size parameters q. As a consequence, one should use materials with much small absorption or realistic materials with optical gain in order to realize such unusual asymptotic properties experimentally. In addition, the radial anisotropy may provide us freedom to investigate extraordinary scattering diagram, near-field energy flux, and Fano resonance of the nanostructures.

ACKNOWLEDGMENTS

[1] L. Rayleigh, Philos. Mag. **41**, 107 (1871).

[2] L. Rayleigh, Philos. Mag. **41**, 274 (1871).

[3] L. Rayleigh, Philos. Mag. **41**, 447 (1871).

[4] J. A. Stratton, *Electromagnetic Theory* (McGraw-Hill, New York, 1941).

[5] M. Kerker, *The Scattering of the Light and Other Electromagnetic Radiation* (Academic Press, New York, 1969).

[6] C. F. Bohren and D. R. Huffman, *Absorption and Scattering of Light by Small Particles* (Wiley, New York, 1998).

[7] H. C. van de Hulst, *Light Scattering by Small Particles* (Dover, New York, 2000).

[8] D. Schurig, J. J. Mock, B. J. Justice, S. A. Cummer, J. B. Pendry, A. F. Starr, and D. R. Smith, Science **314**, 977 (2006).

[9] U. Leonhardt, Science **312**, 1777 (2006).

[10] M. Husnik, M. W. Klein, N. Feth, M. Konig, J. Niegemann, K. Busch, S. Linden, and M. Wegener, Nature Photon. **2**, 614 (2008).

[11] H. Chew and M. Kerker, J. Opt. Soc. Am. **66**, 445 (1976).

[12] Z. Liu, Z. F. Lin, and S. T. Chui, Phys. Rev. E **69**, 016619 (2004).

[13] A. E. Miroshnichenko, Phys. Rev. A **80**, 013808 (2009).

[14] M. I. Tribelsky and B. S. Lukýanchuk, Phys. Rev. Lett. **97**, 263902 (2006).

[15] B. S. Lukýanchuk and V. Ternovsky, Phys. Rev. B **73**, 235432 (2006).

[16] Z. C. Ruan and S. H. Fan, Phys. Rev. Lett. **105**, 013901 (2010).

[17] Z. C. Ruan and S. H. Fan, Appl. Phys. Lett. **98**, 043101 (2011).

[18] L. Verslegers, Z. F. Yu, Z. C. Ruan, P. B. Catrysse, and S. H. Fan, Phys. Rev. Lett. **108**, 083902 (2012).

[19] A. A. Lucas, L. Henrard, and P. Lambin, Phys. Rev. B **49**, 2888 (1994).

[20] L. Gao and X. P. Yu, Phys. Lett. A **335**, 457 (2005).

[21] J. B. Pendry, D. Schurig, and D. R. Smith, Science **312**, 1780 (2006).

[22] T. Ambjornsson, G. Mukhopadhyay, S. P. Apell, and M. Kall, Phys. Rev. B **73**, 085412 (2006).

[23] L. Gao and X. P. Yu, Eur. Phys. J. B **55**, 403 (2007).

[24] C. W. Qiu, L. Gao, J. D. Joannopoulos, and M. Soljacic, Laser Photon. Rev. **4**, 268 (2010).

[25] L. Gao, T. H. Fung, K. W. Yu, and C. W. Qiu, Phys. Rev. E **78**, 046609 (2008).

[26] Y. D. Yin, L. Gao, and C. W. Qiu, J. Phys. Chem. C **115**, 8893 (2011).

[27] M. Kociak, O. Stephan, L. Henrard, V. Charbois, A. Rothschild, R. Tenne, and C. Colliex, Phys. Rev. Lett. **87**, 075501 (2001).

[28] D. Taverna, M. Kociak, V. Charbois, and L. Henrard, Phys. Rev. B **66**, 235419 (2002).

[29] X. P. Yu and L. Gao, Phys. Lett. A **359**, 516 (2006).

[30] Y. J. Huang, W. T. Lu, and S. Sridhar, Phys. Rev. A **77**, 063836 (2008).

[31] Y. W. Jin, D. L. Gao, and L. Gao, PIER **106**, 335 (2010).

[32] R. W. Ziolkowski and E. Heyman, Phys. Rev. E **64**, 056625 (2001).

[33] J. S. Wei and M. F. Xiao, Opt. Commun. **270**, 455 (2007).

[34] Y. Wu, J. S. Li, Z. Q. Zhang, and C. T. Chan, Phys. Rev. B **74**, 085111 (2006).

[35] Y. X. Ni, L. Gao, A. E. Miroshnichenko, and C. W. Qiu, Opt. Lett. **37**, 3390 (2012).